Article

Analysis of the Influencing Factors of Aerostatic Bearings on Pneumatic Hammering

Yifei Li *, Weiping Huang and Ran Sang

School of Civil and Transportation Engineering, Qinghai Minzu University, Xining 810001, China; 13551799580@163.com (W.H.); qhmusrsr@163.com (R.S.)
* Correspondence: liyifei@buaa.edu.cn

Abstract: In this study, in order to reveal the influence mechanism of bearing parameters on pneumatic hammering, an aerostatic bearing with a multi-orifice-type restrictor is analyzed. Firstly, the flow field is investigated, and the vortex-induced excitation is discussed in both the frequency and time domains. Then, the frequency-related displacement impedance is analyzed, and the effects of vortex-induced excitation on pneumatic hammering are discussed. Experiments are also conducted for verification. Moreover, the influence of damping on pneumatic hammering is identified. The results show that with larger damping, the risk of pneumatic hammering can be reduced. Finally, the impacts of design parameters on the damping are discussed in detail using an approximate model. Design optimization is considered to achieve the maximum damping, i.e., the minimum risk of pneumatic hammering. The results show that both the air supply pressure and the pocket volume should be minimized. The analysis process provides a reference for the design of bearings to reduce pneumatic hammering.

Keywords: aerostatic bearing; pneumatic hammering vibration; orifice-type restrictor; damping; numerical simulation

1. Introduction

Due to their high movement precision, low friction, and low heat generation properties, aerostatic bearings have become core components of high-speed machine tools. The operational stability of a bearing has a significant influence on the performance of ultra-precision facilities. However, compared with the common hydrostatic bearing, the operational stability of an aerostatic bearing can be significantly weakened when pneumatic hammering vibration occurs. In such a situation, both the vibration and the operating noise are aggravated. Hence, pneumatic hammering should be suppressed during its design; moreover, the influencing factors of the occurrence of pneumatic hammering should be investigated first.

Pneumatic hammering vibration is a kind of self-excited vibration that can introduce challenges into the stable operation of aerostatic bearings. Micro-vibration and pneumatic hammering vibration commonly occur when a bearing is in operation. Micro-vibration is induced by the vortex flow in the bearing clearance; the vortex flow leads to a pressure fluctuation and then induces micro-vibration [1–4]. Pneumatic hammering is generally induced by an asynchronous change in the motion of the floating facility, the pressure, and the mass flow rate of the gas; moreover, pneumatic hammering is especially prone to occur when an air pocket exists. Both the shape and the volume of the air pocket have a significant influence on the performance of aerostatic bearings [5,6]. The bearing parameters have significant effects on pneumatic hammering vibration. Ye et al. [7] reported that the pocket volume had a direct influence on pneumatic hammering; once the air pocket was removed, the pneumatic hammering ceased. The air supply pressure is also a key issue in the induction of pneumatic hammering [8]. Talukder et al. [9] reported that with an increase in the air supply pressure, pneumatic hammering was more prone to appear. Pneumatic hammering causes more serious vibration and damage than micro-vibration;

hence, it should be reduced at the bearing design stage. For this reason, the rule of the bearing parameter's influence on the characteristics of pneumatic hammering should be determined; moreover, both the excitation source and dynamic characteristics of the bearing should be investigated. However, although the existing research indicates that bearing parameters have a significant influence on pneumatic hammering, their quantitative relationship has not yet been identified. On the other hand, stiffness, damping, and displacement impedance also significantly affect the bearing's dynamic behavior; however, with the improvement of its performance factors, the operation stability of the bearing can be enhanced. The dynamic characteristics and the influence of dynamic performance factors on pneumatic hammering have been studied and discussed by Boffey et al. [10]. Their results indicated that performance factors such as the stiffness and damping of the air film have a direct effect on pneumatic hammering. Currently, the air film is equivalent to a spring-damping system in dynamic analysis, and the frequency-related stiffness and damping of the air film are of particular concern [11]. An aerostatic bearing was considered by Bhat et al. [12], and the stiffness and damping of it were solved; the effects of bearing parameters on stiffness and damping were discussed. An ESA-CFD combined method was proposed by Li et al. for calculating the stiffness and damping of an aerostatic journal bearing [13]. In Chen's research, stiffness and damping were solved by applying a CFD (computational fluid dynamics) simulation [14], and the accuracy of the numerical simulation was verified by conducting experiments [15]. A dynamic performance factor analysis of the bearing system is crucial for revealing the mechanism of micro-vibration or pneumatic hammering; for example, the results of a study showed that the influence of displacement impedance on micro-vibration was significant [16]. Pneumatic hammering vibration is a kind of self-excited vibration; hence, the stability of the system is determined by energy dissipation [17]. As a result, damping performance certainly plays an important role in the occurrence of pneumatic hammering. Furthermore, the influence of the excitation source on pneumatic hammering should be considered, e.g., the influence of vortex-induced excitation (VIE). However, the influence rules of the design parameters and the dynamic performance factors that determine the occurrence of pneumatic hammering have not yet been discussed; therefore, suppressing or reducing pneumatic hammering vibration through parameter design is currently difficult. Thus, the influence of bearing parameters, dynamic performance factors, and VIE on pneumatic hammering should be studied; furthermore, a proper design strategy should be proposed to suppress pneumatic hammering vibration.

In this study, an aerostatic bearing with a multi-orifice-type restrictor is considered. Firstly, the characteristics of VIE and the influence of the vortex flow on pneumatic hammering are discussed. Displacement impedance is considered by analyzing the influence of VIE, and pneumatic hammering is investigated experimentally. To determine the self-excited attribute of pneumatic hammering, the damping performance of the bearing is investigated in detail, as damping acts as an energy dissipater in a self-excited vibration system. Finally, optimization is considered for several cases with different excitation frequencies to further investigate the effects of the bearing parameters on pneumatic hammering.

2. Geometry and Numerical Modeling of an Aerostatic Bearing

An aerostatic thrust bearing with a multi-orifice-type restrictor is depicted in Figure 1. The bearing parameters include the bearing's external diameter D_{out}, internal diameter D_{in}, orifice diameter d, pocket diameter U, pocket depth V, the position of the orifice R, the air film thickness h, the orifice length L, and the air supply pressure P_s. There are 12 orifice-type restrictors along the circumference. The case of a cylindrical air pocket was considered. In the analysis, D_{out} was 80 mm, D_{in} was 48 mm, and L was 0.5 mm. Other parameters were considered as variables that satisfy the following ranges: U(1.5 mm, 2.5 mm), V(0.05 mm, 0.15 mm), R(26 mm, 36 mm), d(0.1 mm, 0.2 mm), h(5 μm, 15 μm), and P_s(0.45 MPa, 0.7 MPa). These bearing parameters have a significant influence on pneumatic hammering. Particularly, the volume of the air pocket and the air supply pressure play

critical roles in the occurrence of pneumatic hammering [7–9]. It is generally believed that to suppress pneumatic hammering, both the air supply pressure and the volume of the air pocket should be reduced [18]. However, the quantitative effect rule of these parameters, which determines pneumatic hammering, has not yet been determined; as a result, optimization of the bearing's design is difficult to achieve.
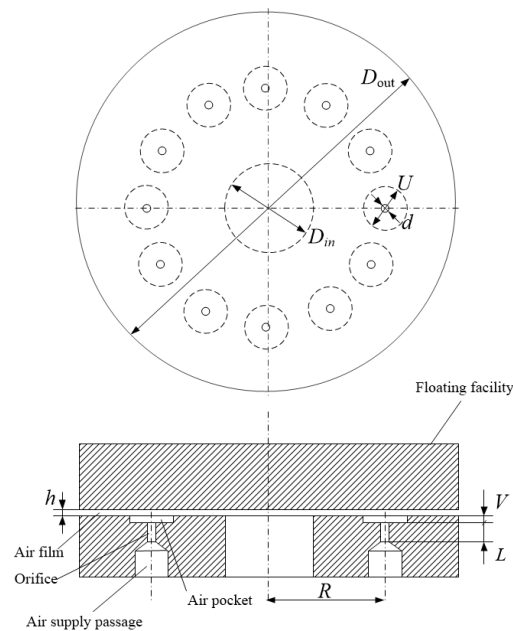
Figure 1. The geometry of an aerostatic thrust bearing with a multi-orifice-type restrictor.

Due to its symmetry, only a 1/12 model was considered in the simulation. Thus, the dynamic performance factors discussed in this article are based on the divided air film component. The inlet of the orifice was considered to be the inlet boundary, and the pressure inlet condition was adopted; the pressure at the inlet position was set as the air supply pressure. The pressure outlet condition was set at the outlet of the air film and the pressure at the outlet was set as the atmosphere pressure. In the adjacent areas with other air film components, the periodic boundary condition was considered. The walls of the orifice, air pocket, and thrust surfaces were all set as walls that satisfy impermeability, adiabaticity, and non-slip conditions. A 3D numerical model was established and the mesh at the orifice position was further refined. Moreover, structured grids were considered. The numerical model and its boundary conditions are shown in Figure 2.
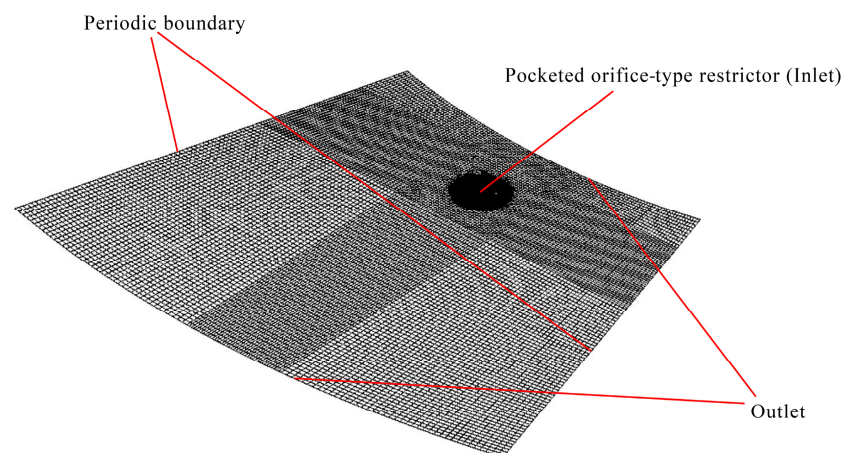
Figure 2. Numerical model and boundary conditions.

In the simulation, the large eddy simulation (LES) method was adopted. The solved governing equations include the following expressions [19]:

$$\frac{\partial \overline{\rho}}{\partial t} + \frac{\partial (\overline{\rho} \widetilde{u}_l)}{\partial x_l} = 0 \tag{1}$$

$$\frac{\partial (\overline{\rho} \widetilde{u}_l)}{\partial t} + \frac{\partial (\overline{\rho} \widetilde{u}_l \widetilde{u}_m)}{\partial x_m} = -\frac{\partial \overline{p}}{\partial x_l} + \frac{\partial \widehat{\sigma}_{lm}}{\partial x_m} + \frac{\partial [\overline{\rho} (\widetilde{u}_l \widetilde{u}_m - \widetilde{u_l u_m})]}{\partial x_m} + \frac{\partial (\overline{\sigma}_{lm} - \widehat{\sigma}_{lm})}{\partial x_m} \tag{2}$$

$$\frac{\partial (\overline{\rho} \widetilde{e} + \overline{\rho} \widetilde{u}_l \widetilde{u}_m / 2)}{\partial t} + \frac{\partial [((\overline{\rho} \widetilde{e} + \overline{\rho} \widetilde{u}_l \widetilde{u}_m / 2 + \overline{p}) \widetilde{u}_m]}{\partial x_j} = \frac{\partial (\widehat{\sigma}_{lm} \widetilde{u}_l)}{\partial x_m} + \frac{\partial \widehat{q}_m}{\partial x_l} + \widehat{A} \tag{3}$$

where $\widehat{\sigma}_{lm}$ can be expressed as follows:

$$\widehat{\sigma}_{lm} = \mu \left(\frac{\partial \widetilde{u}_l}{\partial x_m} + \frac{\partial \widetilde{u}_m}{\partial x_l} \right) \tag{4}$$

$\widehat{q}_m$ can be expressed as follows:

$$\widehat{q}_m = -\lambda \frac{\partial T}{\partial x_m} \tag{5}$$

and $\widehat{A}$ can be expressed as follows:

$$\widehat{A} = \widetilde{u}_l \frac{\partial [\overline{\rho} (\widetilde{u}_l \widetilde{u}_m - \widetilde{u_l u_m})]}{\partial x_m} + \frac{\partial [\overline{e u_m} - \overline{e} \widetilde{u}_m]}{\partial x_m} - \left[\overline{p \frac{\partial u_m}{\partial x_m}} - \overline{p} \frac{\partial \widetilde{u}_m}{\partial x_m} \right] + \left[\overline{\sigma_{lm} \frac{\partial u_l}{\partial x_m}} - \overline{\sigma}_{lm} \frac{\partial \widetilde{u}_l}{\partial x_m} \right]$$
$$+ \frac{\partial (\overline{\sigma}_{lm} \widetilde{u}_i - \widehat{\sigma}_{lm} \widetilde{u}_l)}{\partial x_m} + \frac{\partial (\overline{q}_l - \widehat{q}_l)}{\partial x_l} \tag{6}$$

In Equations (1)–(6), u means the gas velocity, p means the pressure, λ is the thermal conductivity coefficient, t means the time, ρ is the gas density, q is the thermal conductivity, x is the coordinate position, σ is the viscous force, μ is the dynamic viscous, and e represents the total energy. l and m represent different directions. The superscript "~" represents the Favre filter, and the superscript "−" represents the spatial filter. The term $\overline{\rho} (\widetilde{u}_l \widetilde{u}_m - \widetilde{u_l u_m})$ in Equation (2) is also called the subgrid stress, which is determined using the LES model [3].

By using numerical simulation, the vortex flow was specifically studied. The displacement impedance of the air-film floating facility system was investigated and the influence rule of the vortex flow on the pneumatic hammering vibration was determined.

3. Flow Field Analysis and Vortex-Excited Properties

In the flow field analysis, a jet flow was detected at the outlet of the orifice. First, the gas flows into the orifice and the boundary layer thickness in the orifice keeps increasing, which reduces the cross-section area of the flow. Then, when the gas enters the air pocket through the orifice, due to the occurrence of the jet flow, the cross-section area is then increased. The former decrease and the latter increase in the flow's cross-section area provide the conditions needed to form a supersonic region. Once the supersonic region is formed, expansion waves and shock waves may appear. When the gas impacts the thrust surface, the vortex flow forms [19]. The Reynolds number is always used to represent the strength of the vortex flow [1,19]. Studies show that the vortex flow is a major cause of micro-vibration [1,2]. This is because when a vortex exists, it can cause pressure fluctuations; hence, the fluctuating load-carrying force (LCF) acts as an external excitation on the thrust surface, and, as a result, micro-vibration occurs. However, even as one of the major sources of external excitation, the influence of the vortex flow on pneumatic hammering vibration has not yet been discussed. To determine this influence mechanism, the properties of VIE are discussed. Moreover, experiments are conducted for verification.

The flow field in the air pocket is shown in Figure 3 for a test case with the following parameters: D_{out} = 80 mm, D_{in} = 48 mm, d = 0.15 mm, V = 0.1 mm, U = 2 mm, h = 10 μm, R = 32 mm, and P_s = 0.6 MPa. The time step size was taken to be 0.00001 s. The figure

shows that the flow varies with time, and a vortex is detected at the inlet position of the air pocket. The pressure fluctuation caused by the vortex flow acts as an external dynamic load, which can induce self-excited vibration.
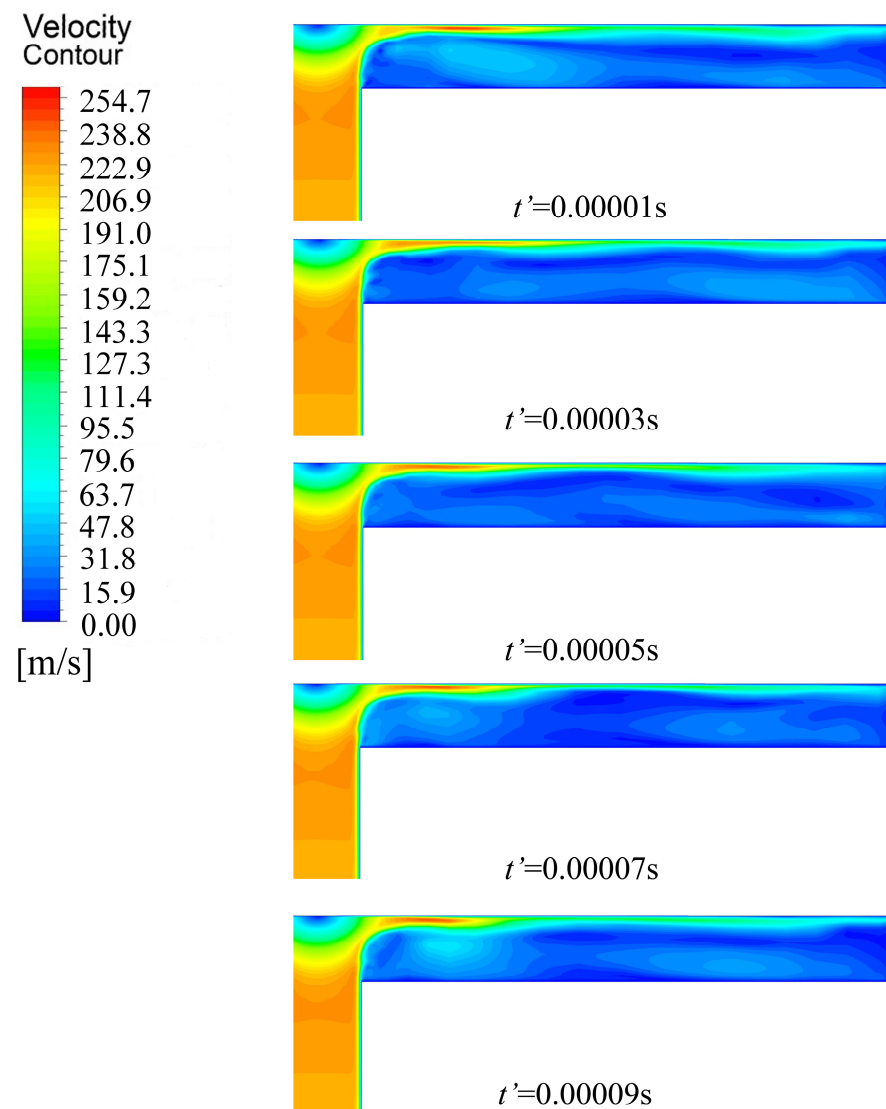
Figure 3. The flow structure in the air pocket.

Excitation characteristics should be studied to determine the influence of the vortex flow on self-excited vibration. The fluctuation of the LCF, as discussed in Figure 3, is shown in Figure 4, where W' represents the fluctuating portion of the LCF. It can be clearly observed that W' fluctuates with time, which suggests an external dynamic excitation.

The frequency properties of VIE should also be investigated. The fast Fourier transform (FFT) method was considered, and amplitude–frequency characteristics were investigated. When the mass of the floating facility is 33.6 Kg, Figures 5–7 show the frequency characteristics of the VIE for the case in which D_{out} = 80 mm, D_{in} = 48 mm, d = 0.15 mm, U = 2 mm, V = 0.1 mm, and R = 32 mm. P_s is taken as 0.5 MPa, 0.6 MPa, and 0.7 MPa in Figures 5–7, respectively.
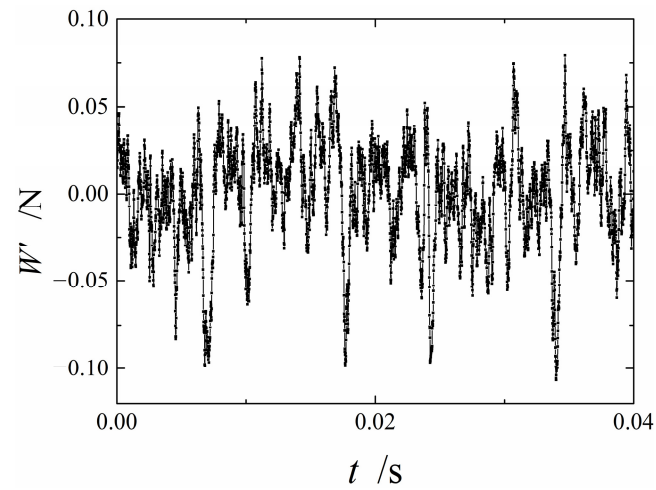
Figure 4. The fluctuation of the LCF with time.
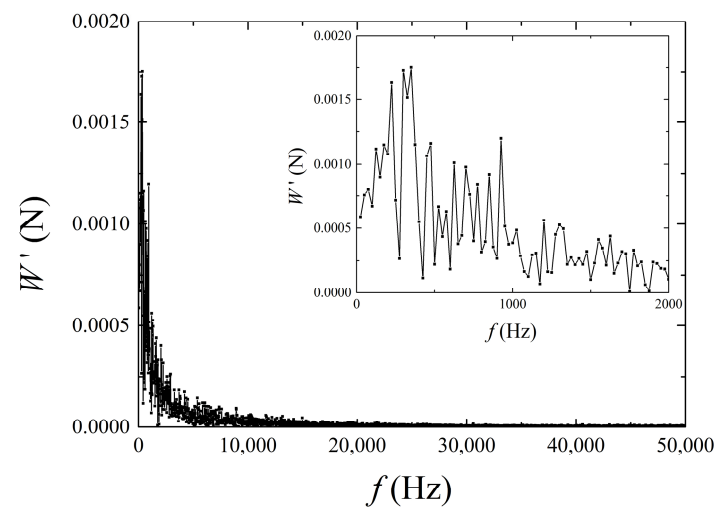
Figure 5. Frequency characteristics of VIE (P_s = 0.5 MPa).
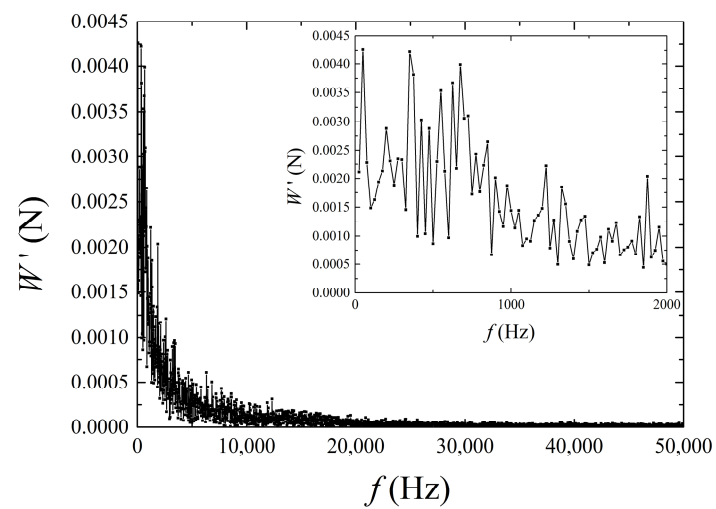
Figure 6. Frequency characteristics of VIE (P_s = 0.6 MPa).
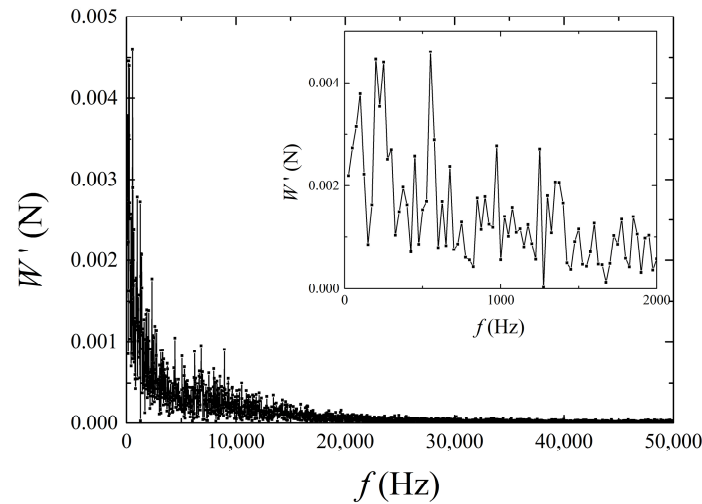
Figure 7. Frequency characteristics of VIE (P_s = 0.7 MPa).

The results of the analysis show that the main frequency range of VIE is low, e.g., 0–10,000 Hz. When the frequency is lower than 2000 Hz, the amplitudes of the components are larger than those when the frequency is higher than 2000 Hz. This result indicates that, to reduce VIE, the low-frequency region, e.g., lower than 2000 Hz, should receive particular focus. As an important excitation source, the effects of the vortex flow on pneumatic hammering have not yet been reported. Hence, to determine its relevance, the frequency characteristics of pneumatic hammering vibration should be discussed and the frequency ranges of VIE and pneumatic hammering vibration should be compared. Moreover, the dynamic properties of the air-film floating facility system should be investigated by focusing on the low-frequency region.

4. The Analysis of the Dynamic Performance Factors of the Bearing System and the Experimental Investigation of Pneumatic Hammering

4.1. The Analysis of the Dynamic Performance of the Bearing

When the bearing is in operation, the pressurized air feeds into the bearing clearance and forms the air film. As previously discussed, the air film is equivalent to a spring-damping system, and a solution for both the stiffness and damping is crucial for the dynamic analysis.

A numerical simulation of the calculation of the stiffness and damping was conducted using the dynamic mesh method. A sinusoidal displacement excitation with a certain frequency was imposed on the thrust surface of the bearing, e.g., $h = h_0 e^{i\omega t}$, where h_0 is the amplitude of the excitation. Moreover, 100 time steps were considered evenly over one time cycle; the smoothing method was used and the spring constant factor was set as 0.1; and the convergence accuracy was set as 10^{-6}. With the input of the displacement excitation, the LCF varies with time. Figure 8 shows the variation in the perturbed LCF F' of the bearing with time when h_0 = 0.1 μm. It can be observed that with different excitation frequencies, both the amplitude and phase angle change.

If the air film is regarded as a spring-damping system, the dynamic equation can be expressed as follows:

$$M\ddot{x} + C\dot{x} + Kx = F_e \tag{7}$$

where M denotes the mass of the floating facility, x is the perturbed displacement, C is the damping, K is the stiffness, and F_e denotes the external perturbed dynamic load. When the harmonic excitation is considered, as discussed in Figure 8, the stiffness and damping of the air film can be calculated based on the relationship between the input displacement excitation and the output LCF.
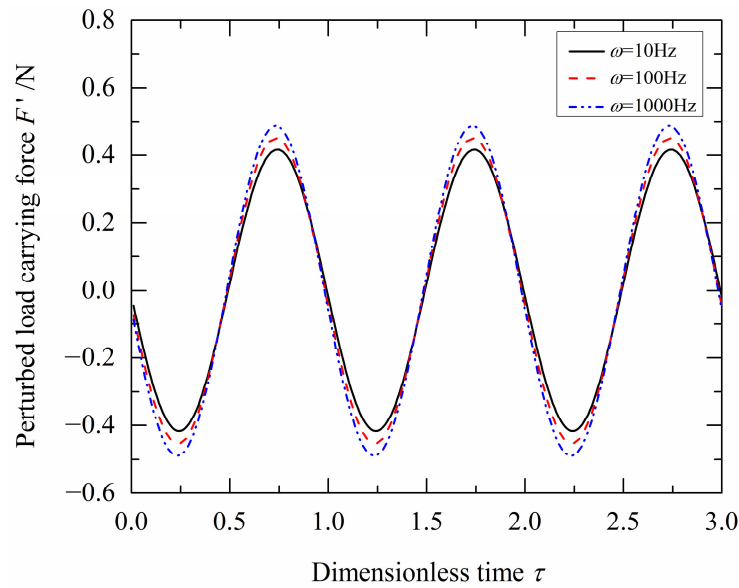
Figure 8. The variation in the perturbed LCF with respect to dimensionless time.

The capability of the vibration system to resist the external dynamic load is an essential factor to discuss. When F_e in Equation (7) denotes the VIE, it can be decomposed using the fast Fourier transform method, and Equation (7) can then be expressed as follows:

$$M\ddot{x} + C\dot{x} + Kx = \sum_{n=1}^{N} F_n e^{i\omega_n t} \tag{8}$$

where F_n is the amplitude and ω_n is the frequency of the nth component. The stiffness and damping depend on the frequency. Accordingly, for the nth component of F_e, it satisfies the following:

$$M\ddot{x} + C(\omega_n)\dot{x} + K(\omega_n)x = F_n e^{i\omega_n t} \tag{9}$$

Thus, x can be expressed as $x = x_n e^{i\omega_n t}$, where x_n is the amplitude of x. As a result, for F_e, the relationship can be represented as follows:

$$M(\sum_{n=1}^{N} x_n e^{i\omega_n t})'' + \sum_{n=1}^{N} [C(\omega_n)(x_n e^{i\omega_n t})'] + \sum_{n=1}^{N} [K(\omega_n)(x_n e^{i\omega_n t})] = \sum_{n=1}^{N} F_n e^{i\omega_n t} \tag{10}$$

Alternatively,

$$\sum_{n=1}^{N} [-M\omega_n^2 + C(\omega_n)\omega_n i + K(\omega_n)]x_n e^{i\omega_n t} = \sum_{n=1}^{N} F_n e^{i\omega_n t} \tag{11}$$

Therefore, x_n can also be represented as follows:

$$x_n = F_n/[K(\omega_n) - M\omega_n^2 + C(\omega_n)\omega_n i] = (F_n/Z_n)e^{i\varphi_n} \tag{12}$$

$$Z_n = \sqrt{[K(\omega_n) - M\omega_n^2]^2 + [C(\omega_n)\omega_n]^2} \tag{13}$$

where Z_n is the displacement impedance and φ_n is the phase angle. x_n becomes smaller when Z_n is larger for a constant F_n. For this reason, Z_n should be enhanced to reduce the influence of the external dynamic load.

The modal frequency of a single-freedom vibration system can be determined by minimizing Z_n [17]. Hence, the influence rules of bearing parameters on Z_n are essential to the dynamic analysis. Due to the "squeeze film" effect, the stiffness and damping of the system both depend on the excitation frequency [13]. As a result, Z_n also varies with the

excitation frequency. To study the modal characteristics of the system, firstly, the stiffness and damping of the air film should be calculated based on the relationship between the excitation and the LCF, as discussed in Figure 8. Once the stiffness and damping are achieved by using the dynamic mesh method, Z_n can be determined through Equation (13). To gain a better understanding of the modal characteristics of the system, the influence rules of bearing parameters on Z_n were discussed.

The displacement impedance and the external excitation characteristics should all be considered in the dynamic analysis. In the numerical calculation of the displacement impedance, the dynamic mesh method was adopted. For the bearing parameters $d = 0.15$ mm, $U = 2$ mm, $V = 0.1$ mm, $R = 32$ mm, and $P_s = 0.6$ MPa, it can be observed, as shown in Figure 9, that the displacement impedance increases largely with the increase in the excitation frequency. This is due to the famous "squeeze film effect". Once the excitation frequency begins to remain at a high level, the thrust surface correspondingly moves up and down fast. However, the gas cannot flow out of the outlet promptly; as a result, the air film becomes stiffer. Hence, the air film possesses an outstanding capability to resist excitation from high frequencies. Thus, the components with high frequencies discussed in Figures 5–7 have little influence on the dynamic behavior of the bearing. However, as previously discussed, the main frequency range of the VIE is low; therefore, the VIE could certainly have an unfavorable influence on the bearing's dynamic behavior. Furthermore, the influence of VIE on the occurrence of pneumatic hammering vibration should be further discussed in terms of the frequency domain.
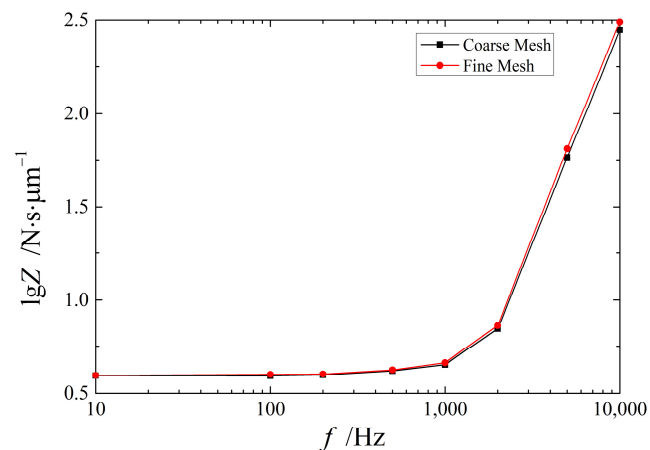
Figure 9. The variation in Z_n with frequency.

The mesh independence verification is shown in Figure 9. For the coarse mesh case, 1 node/μm was considered along the air film, and for the fine mesh case the node density was two times that of the coarse mesh case. Figure 9 shows that the difference between the two cases is rather small; thus, the simulation can be considered to be mesh-independent.

In the dynamic analysis of the aerostatic bearing, the external excitation and the dynamic performance factors of the bearing system should both be considered. With a stable supply of high-pressure gas, the pneumatic hammering vibration is considered to be a kind of self-excited vibration. For self-excited vibration systems, the input and the dissipation of the energy are critical in determining the stability of the system. When the dissipation becomes larger than the input energy, the system can be considered to be stable. For this reason, the analysis of the system's energy dissipation characteristics becomes a core issue.

Damping is present in all vibration systems, and its effect is the removal of energy from the system. Energy dissipation can be determined under conditions of cyclic oscillations as follows:

$$W_d = \oint F_d dx \qquad (14)$$

where F_d denotes the damping force. For the harmonic vibration mode, the energy dissipation W_d can be achieved as $\pi C \omega X^2$, where X is the amplitude of the vibration. Hence, it can be observed that damping can be used to measure the strength of the energy dissipation. For a self-excited vibration system, the larger the damping, the more stable the system becomes. Therefore, the damping performance should be considered during bearing design to reduce pneumatic hammering.

4.2. Experimental Investigation

To gain a further understanding of the frequency properties of pneumatic hammering vibration, experiments were conducted. The experimental apparatus is shown in Figure 10, where the spindle is set vertically, and an aerostatic thrust bearing with a multi-orifice-type restrictor is placed at the bottom of the spindle. The bearing configuration is presented in Figure 1, and the bearing parameters include D_{out} = 80 mm, D_{in} = 48 mm, d = 0.15 mm, U = 2 mm, V = 0.1 mm, and R = 32 mm. The mass of the spindle is 33.6 Kg. Different P_s were considered, from 0.4 MPa to 0.7 MPa, to observe the occurrence of pneumatic hammering. Acceleration sensors were assigned to record the acceleration data in the axial direction, and the sensitivity of the sensors was 4.71 mV/m/s^2.
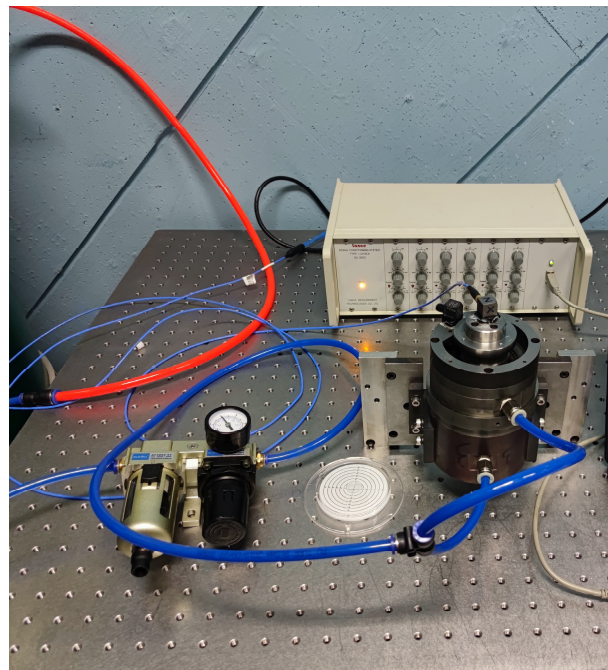
Figure 10. The experimental apparatus.

When the air supply pressure reaches 0.6 MPa, the vibration of the floating facility increases notably, which indicates the occurrence of pneumatic hammering. Figure 11a shows the experimentally achieved vibration acceleration a when P_s = 0.6 MPa and Figure 11b shows the vibration characteristics in the frequency domain.

The experimental results show that the frequencies of the main components of the acceleration are concentrated from 300 to 400 Hz, which means that the frequency of the acceleration of the pneumatic hammering vibration is low. Compared with Figure 6, it can be observed that the main frequency range of the pneumatic hammering vibration is in accordance with that of the VIE, which implies that VIE is a prominent inducing factor of pneumatic hammering. Due to the frequency characteristics of both pneumatic hammering and VIE, the dynamic performance of the system at low frequencies, e.g., lower than 2000 Hz, should receive greater focus.

(a)

(b)
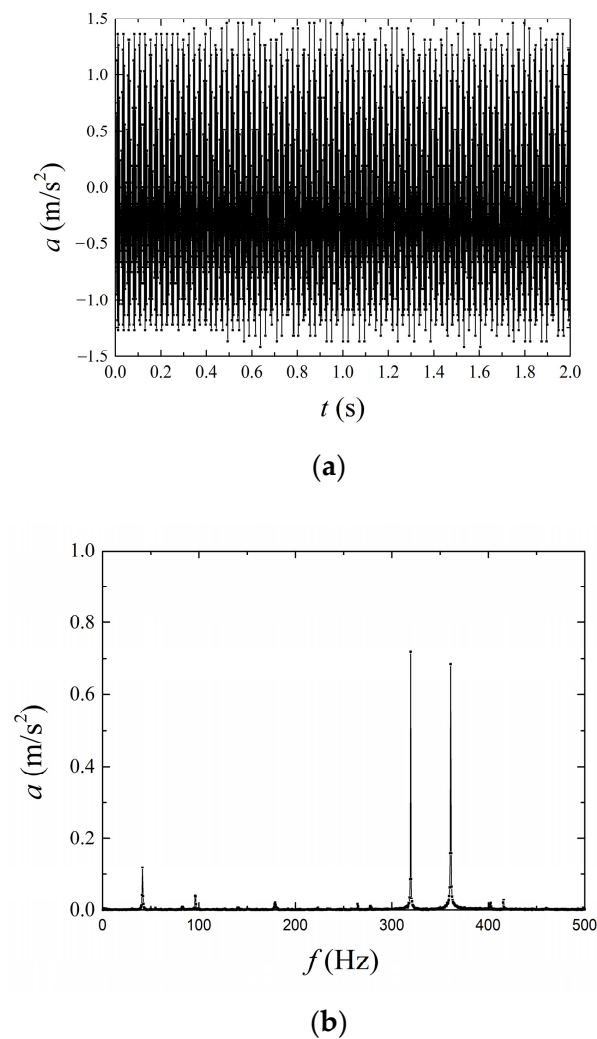
Figure 11. The experiment results. (**a**) The experimentally achieved pneumatic hammering vibration acceleration. (**b**) The experimentally achieved frequency properties of the pneumatic hammering vibration acceleration.

As previously discussed, damping performance is essential in studying the dissipation of energy of a self-excited vibration system. Thus, the damping of the cases discussed in the experiment was numerically calculated by using the dynamic mesh method, and the results are shown in Figure 12.
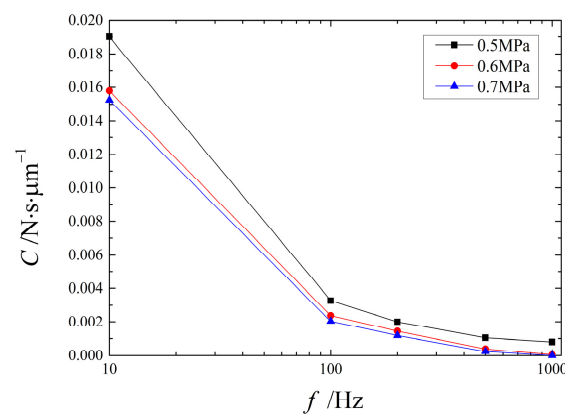
Figure 12. Variation in damping with respect to frequency.

It can be observed in this figure that when the air supply pressure increases, the damping decreases for the different excitation frequencies. Figures 5–7 also show that the amplitude of the components at low frequencies increases from 0.5 MPa to 0.7 MPa, which is due to the increase in the Reynolds number at the inlet of the air pocket. Meanwhile, the damping decreases when the P_s increases from 0.5 MPa to 0.7 MPa. The results of the experiments show that pneumatic hammering only occurs when the air supply pressure reaches 0.6 MPa. Hence, it can be concluded that damping plays a critical role in the occurrence of pneumatic hammering. With larger damping, the energy dissipation becomes larger and the vibration system becomes more stable. Hence, to study the characteristics of pneumatic hammering, it is necessary to first investigate the effects of bearing parameters on damping.

5. The Damping Performance of the Air Film

Previous studies indicate that pneumatic hammering vibration tended to occur when a high air supply pressure and a large pocket volume were adopted [7–9]. However, the quantitative influence rule of the bearing parameters on pneumatic hammering has not yet been discussed. As previously mentioned, the damping performance plays an important role in the dissipation of energy, and, for this reason, the damping can certainly influence the characteristics of pneumatic hammering vibration. Hence, the influences of the design parameters on damping should be discussed first.

To study the influence mechanism of bearing parameters on damping, an approximate model of the damping was established. The considered parameter ranges were as follows: P_s(0.45 MPa, 0.7 MPa), U(1.5 mm, 2.5 mm), V(0.05 mm, 0.15 mm), R(26 mm, 36 mm), d(0.1 mm, 0.2 mm), h(5 μm, 15 μm), and ω(10 Hz, 2000 Hz). The RBF (Radial Basis Functions) method was adopted as described in [13]. A mathematical model of the damping represented by bearing parameters with a high fitting accuracy was achieved. In establishing the approximate model, the layout $L_{121}(11^7)$ was considered based on the orthogonal experimental design used for sample-taking. The R_a^2 factor was considered for verifying the fitting accuracy, and it should be larger than 0.9. Once the approximate model was established, the influence of bearing parameters on damping was investigated intuitively. In addition, the approximate model of the static load-carrying capacity W was also established for the design's optimization, and the considered parameters include P_s, U, V, R, d, and h.

Figures 13–16 show the effect of bearing parameters on damping performance, and two types of air pockets with different volumes are compared. The small pocket sizes include $U = 1.5$ mm and $V = 0.05$ mm. The large pocket sizes include $U = 2.5$ mm and $V = 0.15$ mm. Firstly, the influence of the air film thickness on the damping is discussed in Figure 13, where $d = 0.15$ mm, $R = 32$ mm, and $P_s = 0.55$ MPa. It can be observed that the damping decreases with the increase in the air film thickness, which is because the increase in the gas volume in the bearing clearance weakens the "squeeze film effect", and then the damping increases. Furthermore, it can be observed that when a larger air pocket is used, the damping is decreased, and the influence mechanism is similar to that of the air film thickness. Hence, it can be concluded that the energy dissipation of the small-air-pocket case is larger than that of the large-air-pocket case; therefore, pneumatic hammering is prone to occur when a larger air pocket is adopted. This conclusion is in accordance with previous studies on pneumatic hammering [7].

Figure 14 shows the variation in the damping with respect to the orifice diameter when $h = 10$ μm, $R = 32$ mm, and $P_s = 0.55$ MPa. It can be observed that the influence of the orifice diameter on the damping is non-monotonic. The orifice diameter has a significant influence on the damping because the gas mass flow rate changes with the orifice diameter. When the orifice diameter is relatively small, the gas mass flow rate increases with the increase in the orifice diameter. However, when the orifice diameter reaches a certain level, a supersonic region may form, causing the choking phenomenon, which restricts a further increase in the gas mass flow rate. The "squeeze film effect" is highly affected by the gas mass flow

rate, and, as a result, the damping is influenced. Hence, a non-monotonic variation rule has been observed. Furthermore, the damping of the small-air-pocket case is larger than that of the large-air-pocket case.
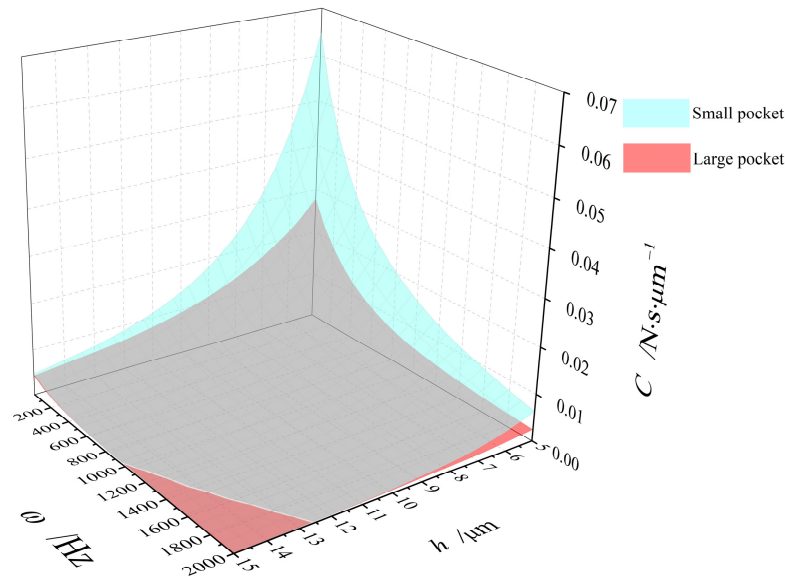
Figure 13. Influence of air film thickness on damping.
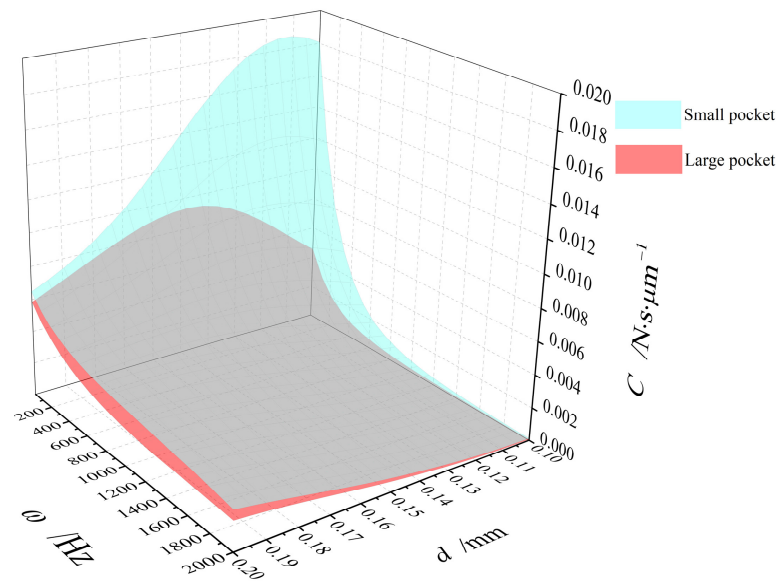
Figure 14. Influence of orifice diameter on damping.

Figure 15 shows the influence of P_s on the damping when $h = 10$ μm, $R = 32$ mm, and $d = 0.15$ mm. The figure shows that with the increase in the air supply pressure, the damping tends to decrease. When the air supply pressure reaches nearly 0.65 MPa, the variation in the damping tends to be flat; this result is also due to the formation of a supersonic region and the choking phenomenon. Generally, the damping decreases when the air supply pressure increases, which indicates that pneumatic hammering is more prone to occur when the air supply pressure is high.

Figure 16 shows the variation in the damping with respect to the orifice position when $h = 10$ μm, $P_s = 0.55$ MPa, and $d = 0.15$ mm. It can be observed that the variation rule of the damping with R for the small-air-pocket case and the large-air-pocket size is different. When the small pocket is used, the damping increases with the increase in the

orifice position; however, when the large pocket is adopted, the damping increases with the decrease in the orifice position. Hence, the optimum orifice position should be determined through design optimization.
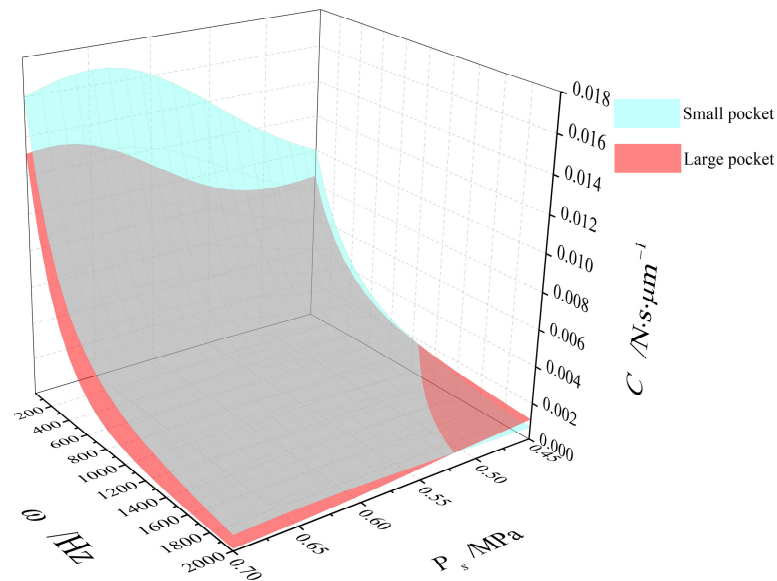
Figure 15. Influence of air supply pressure on damping.
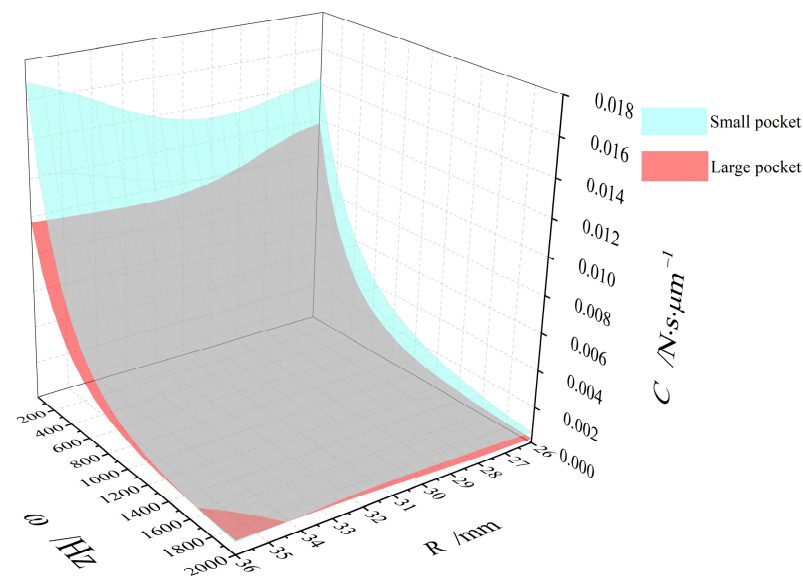
Figure 16. Influence of orifice position on damping.

For all cases discussed in Figures 13–16, the damping decreases with the increase in the excitation frequency or the air pocket volume. The influences of these parameters on damping are highly dependent on the "squeeze film effect". Commonly, with a smaller pocket volume, lower air supply pressure, and smaller air film thickness, the damping becomes larger, which indicates that the risk of pneumatic hammering is reduced. This conclusion is in accordance with findings from experiments discussed in previous studies [7–9].

6. The Optimization of the Damping Performance

To further investigate the effects of bearing parameters on damping performance, design optimization was considered. The optimization of the design is effective in achieving the optimum bearing performance [20,21]. The optimization parameters include P_s, U, V, d,

and R. The mass of the floating facility is 33.6 Kg. The damping varies with the excitation frequency, as discussed in Section 5, and the frequency of VIE is commonly low. Hence, several different frequency points are considered, from 10 Hz to 800 Hz, to investigate the change rule of the optimum combination of bearing parameters. The mathematical model of optimization was established as follows:

$$\begin{aligned} \max\ &C(\boldsymbol{y}) \\ \text{s.t.}\ &W = W_{given} \\ &\omega = \omega_{given} \\ &\boldsymbol{y} \in \boldsymbol{E} \end{aligned} \tag{15}$$

where W_{given} is the given bearing load, ω_{given} is the frequency, and $\boldsymbol{y}$ is the design variable vector that can be expressed as (P_s, U, V, R, d). $\boldsymbol{E}$ is the feasible design field and the ranges of the optimization parameters in $\boldsymbol{E}$ include P_s(0.45 MPa, 0.7 MPa), U(1.5 mm, 2.5 mm), V(0.05 mm, 0.15 mm), R(26 mm, 36 mm), and d(0.1 mm, 0.2 mm). The optimization was conducted based on the approximate model established in Section 5. Because the damping depends on the excitation frequency, as discussed in Section 5, the excitation at low frequencies should also receive greater focus, as mentioned in Section 4. Hence, a total of five cases of excitation frequency ω_{given} were considered in the optimization, which include 10 Hz, 100 Hz, 200 Hz, 500 Hz, and 800 Hz. The considered frequency points were within the frequency range discussed in Section 3. In each case of optimization, one of the frequency points was considered and the optimization constraint $\omega = \omega_{\text{given}}$ was adopted. Through optimization, the change rule of the optimum combination of the bearing parameters was studied. Moreover, the bearing load was balanced by the static load-carrying force, and hence the design constraint $W = W_{\text{given}}$ was considered. The floating facility was supported by the air film, as depicted in Figures 1 and 10, so the gravity of the floating facility was considered as the given bearing load. The air film thickness varied with the given bearing load at different design points. The NLPQL algorithm was adopted in the optimization, and the optimization results are shown in Table 1.

Table 1. Optimization results.

ω/Hz	P_s/MPa	U/mm	V/mm	d/mm	R/mm	C/N·s·µm^{-1}
10	0.45	1.5	0.05	0.1	36	0.0165
100	0.45	1.5	0.05	0.1	36	0.0126
200	0.45	1.5	0.05	0.1	36	0.0079
500	0.45	1.5	0.05	0.1	36	0.0035
800	0.45	1.5	0.05	0.104	36	0.0023

It can be observed from Table 1 that for different excitation frequencies, the air supply pressure, pocket diameter, and depth approach their minimum boundaries, while the orifice position reaches its upper boundary. The orifice diameter also comes close to its lower boundary. For each case, the combination of the optimum parameters has the same change tendency. The results indicate that to achieve maximum damping, the air supply pressure, air pocket volume, and orifice diameter should be minimized and the orifice position should be maximized. Correspondingly, the pneumatic hammering vibration is reduced.

7. Conclusions

In this study, the influencing factors of pneumatic hammering vibration in aerostatic bearings were discussed. Some conclusions can be drawn, which are as follows.

The displacement impedance of the bearing increases with the excitation frequency, which means that the air film has a good ability to resist external dynamic loads with high frequencies. However, the main frequency range of VIE is low, and the main frequency

range of pneumatic hammering vibration is in accordance with that of VIE. This result indicates that VIE acts as a prominent inducing factor of pneumatic hammering vibration.

Pneumatic hammering vibration is a kind of self-excited vibration. Damping plays an important role in the stable operation of the system. The larger the damping, the harder it is for pneumatic hammering vibration to occur, and the more stable the system becomes. For this reason, it is imperative to improve damping through design optimization to reduce pneumatic hammering vibration.

The optimization results show that when a small air supply pressure and air pocket volume are applied, the damping tends to become larger. This result indicates that pneumatic hammering vibration is reduced under such conditions. The influences of the orifice diameter and the orifice position are non-monotonic, which means that the optimum combination of bearing parameters should be achieved through design optimization.

References

1. Chen, X.D.; Chen, H.; Luo, X.; Ye, Y.X.; Hu, Y.T.; Xu, J.Q. Air vortices and nano-vibration of aerostatic bearings. *Tribol. Lett.* **2011**, *42*, 179–183. [CrossRef]
2. Zhu, J.C.; Chen, H.; Chen, X.D. Large eddy simulation of vortex shedding and pressure fluctuation in aerostatic bearings. *J. Fluid Struct.* **2013**, *40*, 42–51. [CrossRef]
3. Li, Y.T.; Zhao, J.Y.; Zhu, H.X.; Lin, Y.X. Numerical analysis and experimental study on the microvibration of an aerostatic thrust bearing with a pocketed orifice-type restrictor. *Proc. IMechE Part J J. Eng. Tri.* **2015**, *229*, 609–623. [CrossRef]
4. Yoshimura, T.; Hanafusa, T.; Kitagawa, T.; Hirayama, T.; Matsuoka, T.; Yabe, H. Clarifications of the mechanism of nano-fluctuation of aerostatic thrust bearing with surface restriction. *Tribol. Int.* **2012**, *48*, 29–34. [CrossRef]
5. Gao, S.Y.; Cheng, K.; Chen, S.J.; Ding, H.; Fu, H.Y. CFD based investigation on influence of orifice chamber shapes for the design of aerostatic thrust bearings at ultra-high speed spindles. *Tribol. Int.* **2015**, *92*, 211–221. [CrossRef]
6. Akhondzadeh, M.; Vahdati, M. Air pocket effects on air spindle vibrations in nanomachining. *Proc. IMechE Part B J. Eng. Manuf.* **2014**, *228*, 328–336. [CrossRef]
7. Ye, Y.X.; Chen, X.D.; Hu, Y.T.; Luo, X. Effects of recess shapes on pneumatic hammering in aerostatic bearings. *Proc. IMechE Part J J. Eng. Tri.* **2010**, *224*, 231–237. [CrossRef]
8. Stowell, T.B. Pneumatic hammer in a gas lubricated externally pressurized annular thrust bearing. *J. Lubr. Technol.* **1971**, *93*, 498–503. [CrossRef]
9. Talukder, H.M.; Stowell, T.B. Pneumatic hammer in an externally pressurized orifice-compensated air journal bearing. *Tribol. Int.* **2003**, *36*, 585–591. [CrossRef]
10. Boffey, D.A.; Waddell, M.; Dearden, J.K. A theoretical and experimental study into the steady-state performance characteristics of industrial air lubricated thrust bearings. *Tribol. Int.* **1985**, *18*, 229–233. [CrossRef]
11. Arghir, M.; Matta, P. Compressibility effects on the dynamic characteristics of gas lubricated mechanical components. *Comptes Rendus Mecanique.* **2009**, *337*, 739–747. [CrossRef]
12. Bhat, N.; Kumar, S.; Tan, W.; Narasimhan, R.; Low, T.C. Performance of inherently compensated flat pad aerostatic bearings subject to dynamic perturbation forces. *Precis. Eng.* **2012**, *36*, 399–407. [CrossRef]
13. Li, Y.F.; Yin, Y.H.; Cui, H.L. An ESA-CFD Combined Method for Dynamic Analysis of the Aerostatic Journal Bearing. *Lubr. Sci.* **2020**, *32*, 387–403. [CrossRef]
14. Chen, X.D.; Zhu, J.C.; Chen, H. Dynamic characteristics of ultra-precision aerostatic bearings. *Adv. Manuf.* **2013**, *1*, 82–86. [CrossRef]
15. Yu, P.L.; Chen, X.D.; Wang, X.L.; Jiang, W. Frequency-dependent nonlinear dynamic stiffness of aerostatic bearings subjected to external perturbations. *Int. J. Precis. Eng. Man.* **2015**, *16*, 1771–1777. [CrossRef]
16. Li, Y.F. Investigation of micro-vibration reduction method based on dynamic performance analysis of aerostatic bearing. *Proc. IMechE Part J J. Eng. Tri.* **2023**, *237*, 2074–2087. [CrossRef]
17. Thomson, W.T.; Dahleh, M.D. *Theory of Vibration with Applications*, 4th ed.; Chapman & Hall: London, UK, 1993.

18. Gao, Q.; Chen, W.Q.; Lu, L.H.; Huo, D.H.; Cheng, K. Aerostatic bearings design and analysis with the application to precision engineering: State-of-the-art and future perspectives. *Tribol. Int.* **2019**, *135*, 1–17. [CrossRef]
19. Li, Y.F.; Yin, Y.H.; Yang, H.; Liu, X.E.; Mo, J.; Cui, H.L. Micro-vibration analysis and optimization of aerostatic bearing with pocketed orifice-type restrictor based on numerical simulation. *J. Appl. Fluid. Mech.* **2018**, *11*, 1115–1124.
20. Wang, G.Q.; Li, W.J.; Liu, G.P.; Feng, K. A novel optimization design method for obtaining high-performance micro-hole aerostatic bearings with experimental validation. *Tribol. Int.* **2023**, *185*, 108542. [CrossRef]
21. Yu, P.L.; Huang, L.; Li, S.Z.; Guo, L.B.; Zhong, M.; Zhang, L.P. Theoretical predictions and experimental measurements of novel aerostatic bearing with multi-inclined-orifice restrictors for the improvement of stability. *Precis. Eng.* **2024**, *88*, 266–278. [CrossRef]